JOURNAL OF GEOPHYSICAL RESEARCH, VOL. 112, A09219, doi:10.1029/2006JA012098, 2007

Low-frequency waves in the foreshock of Saturn: First results from Cassini

C. Bertucci,[1] N. Achilleos,[1] C. Mazelle,[2] G. B. Hospodarsky,[3] M. Thomsen,[4] M. K. Dougherty,[1] and W. Kurth[3]

Received 23 September 2006; revised 11 April 2007; accepted 24 May 2007; published 29 September 2007.

[1] We present the first characterization of low-frequency upstream waves associated with Saturn's foreshock from observations by the Cassini spacecraft. A classification based on their frequency in the spacecraft frame (s/c) yields two groups: (1) a large majority of waves with frequencies below the local proton cyclotron frequency Ω_{H+} and (2) waves with frequencies above Ω_{H+}. The waves within the first group are usually phase steepened and have a left-hand polarization in the spacecraft frame. In addition, they present left-hand-polarized (s/c) dispersive wave packets attached to the steepening front. An analysis of these waves suggests that these are sunward propagating ion/ion resonant right-hand mode waves that steepen and emit a whistler precursor to stop the steepening. These waves seem to populate the deep ion foreshock. Within the second group we find quasi-monochromatic and steepened waves with a right-hand polarization (s/c). Among the first we find noncompressive and slightly compressive waves, whereas the steepened ones are very compressive, show oblique propagation, and also display dispersive wave packets. Assuming that these packets are also whistlers, we suggest that these waves could be generated by the ion/ion resonant left-hand mode. Then, during the nonlinear regime they would become compressive and eventually steepen, emitting a whistler precursor. However, we are unable to provide evidence for hot ion beams that could be related to this instability. This is the first time that such waves are observed at Saturn, and observations confirm that these waves contribute to Saturn's quasi-parallel shock reformation.

Citation: Bertucci, C., N. Achilleos, C. Mazelle, G. B. Hospodarsky, M. Thomsen, M. K. Dougherty, and W. Kurth (2007), Low-frequency waves in the foreshock of Saturn: First results from Cassini, *J. Geophys. Res.*, *112*, A09219, doi:10.1029/2006JA012098.

1. Introduction

[2] The extensive exploration of the Earth's foreshock region has led to an understanding of the structure which may be expected in similar regions at the outer planets. The foreshock is the region in the upstream space which is magnetically connected to the bow shock. Because of this property of the foreshock, it is possible for particles from the incident solar wind in this region to coexist with a second population of particles which "backstream" from the bow shock [*Asbridge et al.*, 1968]. Such particles may originate from several possible sources: (1) solar wind ions and electrons specularly reflected at the bow shock, (2) solar wind particles reflected by magnetic mirroring or scattered by MHD waves, and (3) magnetosheath particles which leak back into the upstream region. In addition to their parallel and perpendicular (cyclotron) motion with respect to the interplanetary magnetic field (IMF) **B**, all particles in the foreshock are accelerated by the solar wind convective electric field **E** and their guiding centers undergo a drift motion in the $\mathbf{E} \times \mathbf{B}$ direction which is the same for all particles. The backstreaming particles are confined in the space between the bow shock and the surface formed by the IMF magnetic field lines tangent to the bow shock. These particles also have spatial distributions that are ordered according to their parallel (field-aligned) velocity components, which leads to the development of an external electron foreshock and an inner ion foreshock.

[3] In situ observations have shown that the structures of the planetary shocks and foreshocks strongly depend on three parameters: the plasma β, the magnetosonic Mach number M_{MS}, and the shock normal angle, θ_{Bn} [*Russell*, 1985]. Under steady upstream conditions, it is the latter that determines the type of backstreaming ion distribution to be found at a given location inside the foreshock. Thus the region magnetically connected to quasi-perpendicular shocks ($45° < \theta_{Bn} < 90°$) is characterized by narrow (beam) distributions whose peaks are aligned with the ambient magnetic field [e.g., *Bonifazi and Moreno*, 1981a] and whose bulk speeds correlate with θ_{Bn} [*Paschmann et al.*, 1980]. Downstream from this region, the backstreaming ion

[1]Space and Atmospheric Physics Group, Imperial College London, London, UK.
[2]Centre d'Etude Spatiale des Rayonnements, CNRS, Université Paul Sabatier, Toulouse, France.
[3]Department of Physics and Astronomy, University of Iowa, Iowa City, Iowa, USA.
[4]Los Alamos National Laboratory, Los Alamos, New Mexico, USA.

0148-0227/07/2006JA012098$09.00

distributions display peaks at nonzero pitch angles. These can be either gyrotropic (rings) or grouped around a given gyrophase as they gyrate around the ambient magnetic field [*Meziane et al.*, 2004]. Further inside the foreshock, upstream from parallel shock, the ion distributions are strongly diffused both in pitch angle and energy [*Bonifazi and Moreno*, 1981b].

[4] The presence of backstreaming particles within the foreshock leads to the generation of electromagnetic waves which are usually noticeable in magnetometer data. The properties of these waves also vary with θ_{Bn}. In the field-aligned beam region, near the ion foreshock boundary, no waves are observed [e.g., *Meziane et al.*, 2004]. Gyrating ion distributions are associated with coherent, nonlinear, low-frequency (LF) waves that propagate sunward at small (but nonzero) angles to the mean magnetic field with a right-hand polarization in the solar wind frame [*Mazelle et al.*, 2003]. The regions with diffuse distributions are usually populated with extremely nonlinear LF waves such as shocklets and short large-amplitude magnetic structures or "SLAMS" [*Russell et al.*, 1971; *Schwartz et al.*, 1992], which contribute to the shock reformation in the quasi-parallel sector [*Schwartz and Burgess*, 1991]. In addition to these, whistler waves at frequencies around 1 Hz in the spacecraft frame [*Russell et al.*, 1971] have been observed in the Earth's foreshock. These do not seem to be unequivocally related to backstreaming ions [*Hoppe et al.*, 1982], but they have been observed with backstreaming electrons [*Feldman et al.*, 1983].

[5] Most of the LF waves observed at the Earth's foreshock propagate sunward with a right-hand polarization in the solar wind frame [*Narita et al.*, 2006], which is perceived as left-hand in the spacecraft frame, as the waves are convected downstream by the supermagnetosonic flow. This ion/ion right-hand resonant mode is the instability with the highest growth rate for a cold, field-aligned beam of backstreaming ions [*Gary*, 1993].

[6] Waves with a right-hand polarization in the spacecraft frame have also been observed in the terrestrial foreshock [e.g., *Schwartz et al.*, 1992; *Eastwood et al.*, 2003]. Their propagation vector being determined from multispacecraft techniques [e.g., *Pinçon and Motschmann*, 1998], most of these waves are interpreted as sunward, parallel propagating Alfvén/ion cyclotron waves [e.g., *Eastwood et al.*, 2003]. This instability, also known as the ion/ion left-hand resonant mode [*Gary*, 1993], is excited in the presence of hot ($V_{thermal} > V_{beam}$) backstreaming ions.

[7] Although the observations at Earth represent a vital element in the study of the physical processes occurring at planetary foreshocks, these occur in a different range in parameter space, as the solar wind properties vary with heliocentric distance.

[8] At Saturn, the IMF is significantly weaker and its mean orientation is expected to be perpendicular to the Saturn/Sun direction. In addition, the solar wind is significantly faster and more tenuous, leading to a higher magnetosonic Mach number ($\langle M_{MS} \rangle \sim 14$ assuming a V_{SW} = 400 km according to *Achilleos et al.* [2006] and a greater convective gyroradius for the reflected ions ($\langle \rho \rangle \sim 12000$ km using V_{SW} = 400 km according to *Achilleos et al.* [2006]. Nevertheless, Saturn's much larger magnetosphere (the Kronian magnetopause's standoff distance is of the order of 20 R_S, where 1 R_S = 60330 km) leads to a more extended interaction region. Finally, the presence of a significant amount of water group ions within Saturn's magnetosphere [*Young et al.*, 2005] originating from the ionization of the E-ring and Enceladus' dynamic atmosphere [*Tokar et al.*, 2006] is a potential source of heavy ion species into the upstream region via leakage [*Thomsen et al.*, 1983].

[9] Before the first detection of foreshock waves at Saturn, *Hoppe and Russell* [1982] found that the frequency of large-amplitude, low-frequency upstream waves increases with the IMF strength following a power law. This suggested not only that such waves are generated from ion cyclotron resonant instabilities generated by the presence of solar wind speculary reflected ions of similar energies, but also that ion resonant waves at further heliocentric distances would tend to occur at lower frequencies. As a result, the access to the high-frequency region of the wave spectrum at planetary foreshocks by typical dc magnetometers improves with heliocentric distance.

[10] The first observations of ion-resonant LF upstream waves at Saturn were reported by *Bavassano-Cattaneo et al.* [1991] from Voyager 1 magnetometer and plasma data during the Saturn flyby in November 1980. In the spacecraft frame, these waves had periods of about 550 s, and an elliptical right and left-hand polarization with respect to the ambient magnetic field. In addition, these waves showed relative amplitudes of typically 0.3 and propagated at 30° with respect to the ambient magnetic field. During these observations, the spacecraft appeared to be magnetically connected to Saturn's bow shock, leading to the interpretation that these waves were associated with the planet's ion foreshock.

[11] Cassini is the first spacecraft devoted to the exhaustive study of Saturn's magnetosphere and its interaction with the solar wind. The Cassini dual magnetometer investigation (MAG) [*Dougherty et al.*, 2004] consists of a vector helium magnetometer (VHM) and a fluxgate magnetometer (FGM) mounted respectively at the end of and halfway along the 11-m spacecraft boom. The FGM provides wide-range (±44,000 nT) fast vector measurements (up to 32 vectors/s), whereas the VHM range is ±256 nT in the vector mode and ±16384 nT in the scalar mode (SHM) with a resolution of 2 s^{-1} and 1 s^{-1}, respectively.

[12] In this paper we present observations of upstream low-frequency (LF) waves at Saturn by the Cassini magnetometer experiment (MAG). The coordinate system to be used throughout will be the Saturn-centered Kronian Solar Orbital (KSO), whose x axis points toward the Sun, the z axis points northward and perpendicular to Saturn's orbital plane with the y completing the orthogonal system. In the next sections we describe several examples of observations by MAG (supported by measurements from other plasma instruments onboard Cassini), and we analyze the properties of the waves in an attempt to identify the mode with which they are associated. However, theoretical considerations on the evolution of these waves during the nonlinear growth phase are beyond the scope of this work.

2. Observations

[13] The observations described here were obtained during the first three orbits of Cassini around Saturn (DOY 149

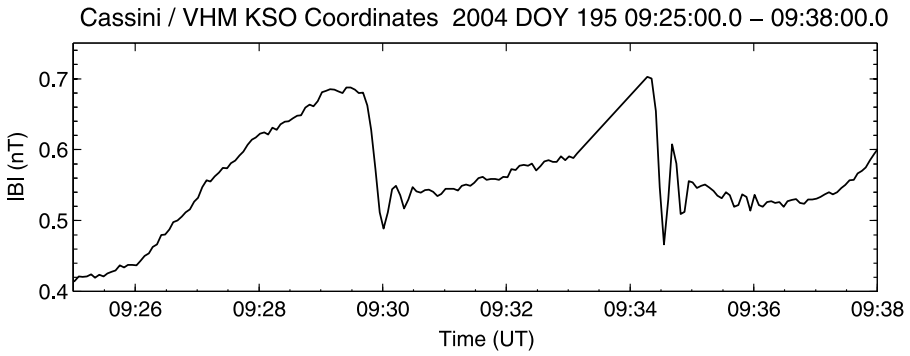

Figure 1. Example of steepened waves at frequencies below Ω_{H+} as seen by the Cassini dual magnetometer investigation (MAG)/vector helium magnetometer (VHM) on 13 July 2004 between 0925:00 and 0938:00 UT. Cassini is located at 81.6 R_S from Saturn and at 5 hours 41 min A.M. LT. In spite of the data gap between 0933:09 and 0934:17, the waves clearly show the presence of a sharp steepening front and a high-frequency wave train on the right of the waveform. KSO, Kronian Solar Orbital.

through 346, 2004). These orbits were located in the dawn sector (between 5 and 8 AM Saturn local time, SLT, where a scale of 0–24 hours corresponds to one planetary rotation), up to a distance of ~140 R_S (1R_S = 60330 km). In agreement with Parker's spiral model, Cassini MAG observations show that the IMF near Saturn usually resides on the ecliptic plane and is perpendicular to the planet-Sun line and the solar wind flow. As a result and according to the location of the bow shock's mean standoff distance around 30 R_S [*Achilleos et al.*, 2006], Cassini was expected to explore Saturn's foreshock downstream from this distance along the Saturn-Sun direction. However, as it will be shown later, the IMF was occasionally parallel to the expected solar wind direction. This particular configuration allowed the exploration of Saturn's deep ion foreshock.

[14] We looked for coherent, low-frequency oscillations in the magnetic field associated with Saturn's foreshock. In absence of a physical model for the Kronian bow shock, we checked for field line connection by using the *Slavin et al.* [1985] hyperboloidal fit (eccentricity: e = 1.71; distance between Saturn center and the surface's focus: X_0 = 6 R_S) varying the semilatus rectum L so as to make the fit coincide with the bow shock crossing at which Cassini was closest to the analyzed wave event.

[15] As a result of this survey, and on the basis of the frequency of the oscillations in the spacecraft frame relative to the local proton cyclotron frequency Ω_{H+}, we identified two distinct types of oscillations: (1) waves with frequencies below Ω_{H+} and (2) waves with frequencies above Ω_{H+}. In sections 2.1 and 2.2, we discuss some specific examples of both types of waves.

2.1. Waves at Frequencies Below Ω_{H+}

[16] The first category of waves has periods of the order of 5 to 10 min in the spacecraft frame (2 to 3 times the local proton cyclotron period for an IMF magnitude between 0.3 and 0.5 nT), and they are the most frequently observed.

[17] Figure 1 shows the first clear example of such oscillations seen by Cassini MAG/VHM between 0925:00 and 0938:00 UT on 13 July 2004. During this interval, Cassini is located at 81.6 R_S from the planet, and at 05:41 A.M. SLT. These oscillations have a "sawtooth" shape with the sharp edge on the right. In spacecraft frame, the period of these oscillations is 270 s, almost 2.5 times the local proton cyclotron period for an ambient magnetic field magnitude of ~0.6 nT. In addition, MAG measurements reveal the presence of packets of quasi-sinusoidal waves attached to the sharper edge of each 270-s oscillation. The period of the oscillations within these packets is on the order of a few tens of seconds, clearly above the local proton cyclotron frequency.

[18] Figure 2 shows another example of such oscillations extracted from a long wave train observed by Cassini MAG/VHM from 14 November 2004 (day 319) 2100 UT to 16 November 2004 (day 321), 0200 UT. Figure 2 shows the B_y component of the magnetic field measured by VHM between 0355 and 0430 UT on 15 November 2004 at 74.6 R_S and 83.5° solar zenith angle (SZA). Four oscillations with a mean period of 493 s are clearly seen. As in the example shown in Figure 1, these waves show clear signatures of phase steepening with the front located at the right of the wave, and a higher-frequency wave packet that appears attached to it.

[19] Figure 3 shows a detail of one of these wave packets as seen in one of the components of the magnetic field. With the leading edge on the left of Figure 3, these wave packets are characterized by two features. The first feature is the decrease in the amplitude of the oscillations within the packet with increasing distance from the front. The second feature is the decrease of the periods of these oscillations, also with increasing distance from the front. Figure 3 also shows the values of consecutive periods, which vary from 33 to 21 s, suggesting the dispersive nature of these packets.

[20] We studied the polarization and the propagation of these waves using minimum variance analysis (MVA). This technique [e.g., *Sonnerup and Schreible*, 1998] provides an estimate of the direction of propagation for a plane wave by calculating the eigenvectors of the covariance matrix of the magnetic field within each interval. Then, the direction of propagation is associated with the eigenvector that corresponds to the minimum eigenvalue λ_3 (the maximum and intermediate eigenvalues are respectively λ_1 and λ_2).

[21] Figure 4 shows the results of the MVA applied on one period of these waves between 0355 and 0400 on

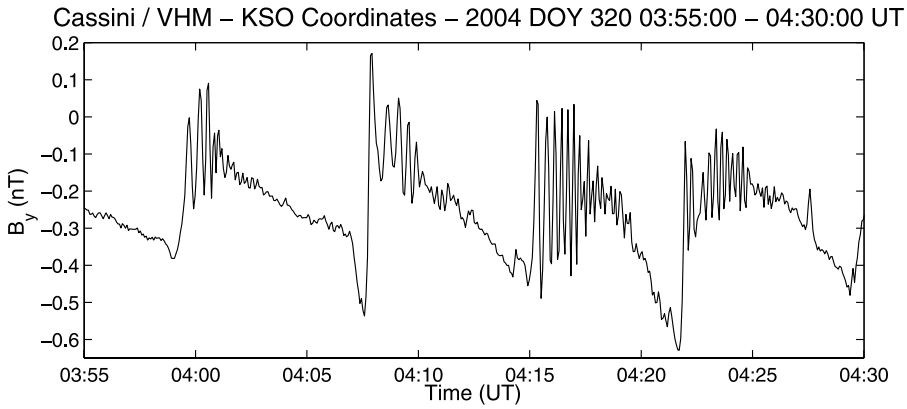

Figure 2. Extract of a long wave train of steepened waves at frequencies below Ω_{H+} detected by MAG/VHM between 0355 and 0430 UT on 15 November 2004 at 74.6 R_S distance and 83.5° solar zenith angle (SZA). Once again, the steepening front is located at the right of the wave with a higher-frequency wave packet attached to it.

15 November (day 320) 2004. Figure 4a shows the components of the magnetic field along the maximum (B_1), intermediate (B_2), and minimum (B_3) variance directions. From left to right, it can be seen how an early linear polarization is followed by a circular polarization toward the end of the interval. This defines a clear minimum variance direction as shown by the large ratio between the intermediate and minimum eigenvalues of the covariance matrix (λ_2/λ_3 = 24.5). The angle between the minimum variance vector and the mean magnetic field suggests that the propagation of these waves is oblique (θ_{kB} = 39.9° ± 1.4°). Figures 4b and 4c show the projection of the wave magnetic field (hodograms) on the intermediate-minimum and the maximum-intermediate variance planes, respectively. The hodogram in Figure 4b shows an extremely low dispersion of the measurements on the minimum variance plane, whereas the hodogram in Figure 4c shows that the wavefield rotation around the minimum variance direction is left-handed with respect to the mean magnetic field. The circle and the asterisk indicate the beginning and the end of the hodogram, respectively.

[22] We also analyzed the polarization of the dispersive wave packets that follow the steepened waves. Figure 5 shows the results of the MVA for the interval 1420:46–1421:44 UT on 15 November (day 320) 2004. Two hodograms show the wave magnetic field in the minimum-intermediate (Figure 5b) and maximum-intermediate (Figure 5c) variance planes in the spacecraft frame. Once again, the high intermediate to minimum eigenvalue ratio, λ_2/λ_3 = 79.9, indicates a very well defined minimum variance vector. The hodogram in Figure 5c shows a left-hand polarization with respect to the mean magnetic field with decreasing amplitude. In addition, the direction of propagation of the high-frequency packet is very close to the mean magnetic field for the interval of analysis: the angle between these two vectors is θ_{kB} = 12.2° ± 0.8°. In spite of the high λ_2/λ_3 ratios, these wave packets always exhibit a compressive component which is correlated to the plasma density, as measured by Cassini's Radio Plasma Wave System (RPWS) [*Gurnett et al.*, 2004] from the Langmuir frequency (Figure 6). Interestingly, the magnetic field orientation at the beginning of the steepened oscillations is recovered after the high-frequency wave train.

[23] In order to investigate the type of ion distribution these waves are associated with, their location with respect to Saturn's foreshock boundary was also studied. In absence of a physical model of the Kronian shock and owing to the lack of a reliable estimation of the solar wind pressure, the position of the foreshock boundary was deduced using Cassini MAG measurements. Assuming that the solar wind

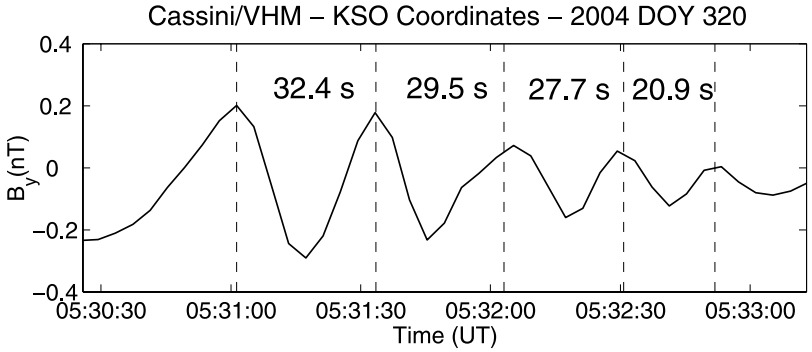

Figure 3. Detail of one of the packets associated with the steepened waves at frequencies below Ω_{H+}. Note the monotonic decrease in amplitude and in the period of the oscillations with increasing distance from the steepening front (located on the left).

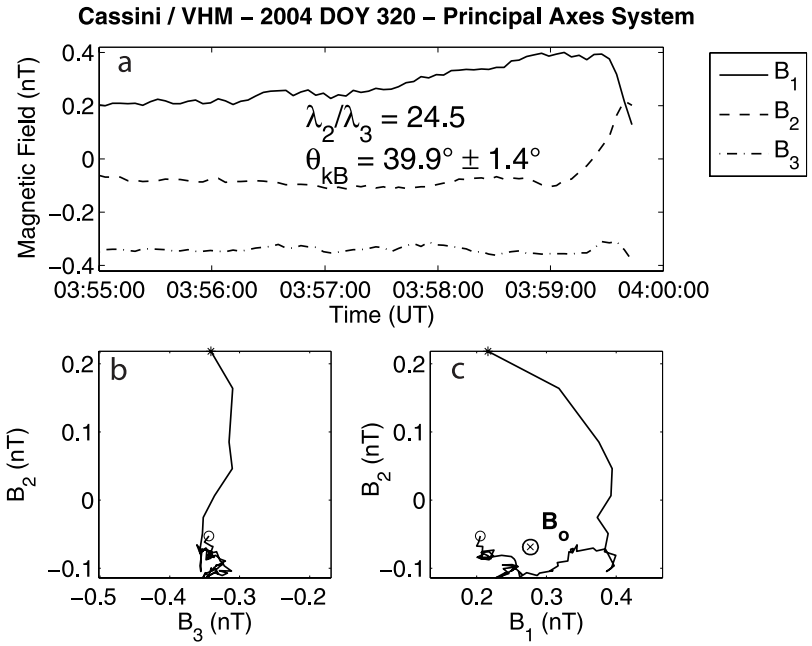

Figure 4. (a) Magnetic field components along the maximum variance direction (solid line), intermediate variance direction (dashed line), and minimum variance direction (dot-dashed line) obtained from the interval 0355 and 0400 UT on 15 November (day 320) 2004. (b) Hodogram showing the magnetic field in the intermediate-minimum variance plane. (c) Hodogram showing the magnetic field in the maximum-intermediate variance plane. The circle and the asterisk indicate the beginning and the end of the hodogram, respectively.

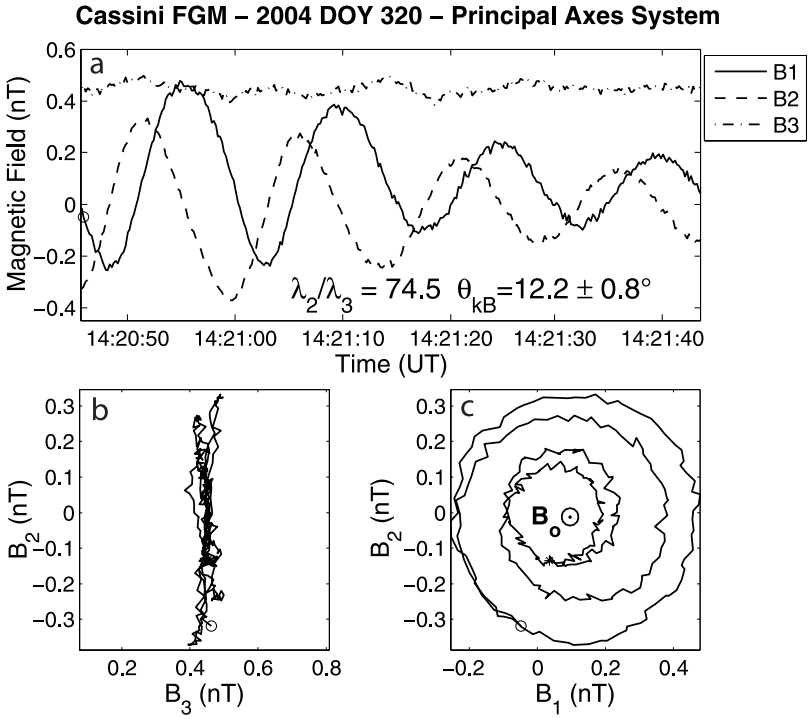

Figure 5. (a) Magnetic field components along the maximum variance direction (solid line), intermediate variance direction (dashed line), and minimum variance direction (dot-dashed line) obtained from the interval 1420:46–1421:44 UT on 15 November (DOY 320) 2004. (b) Hodogram showing the magnetic field in the intermediate-minimum variance plane. (c) Hodogram showing the magnetic field in the maximum-intermediate variance plane. The circle and the asterisk indicate the beginning and the end of the hodogram, respectively. FGM, fluxgate magnetometer.

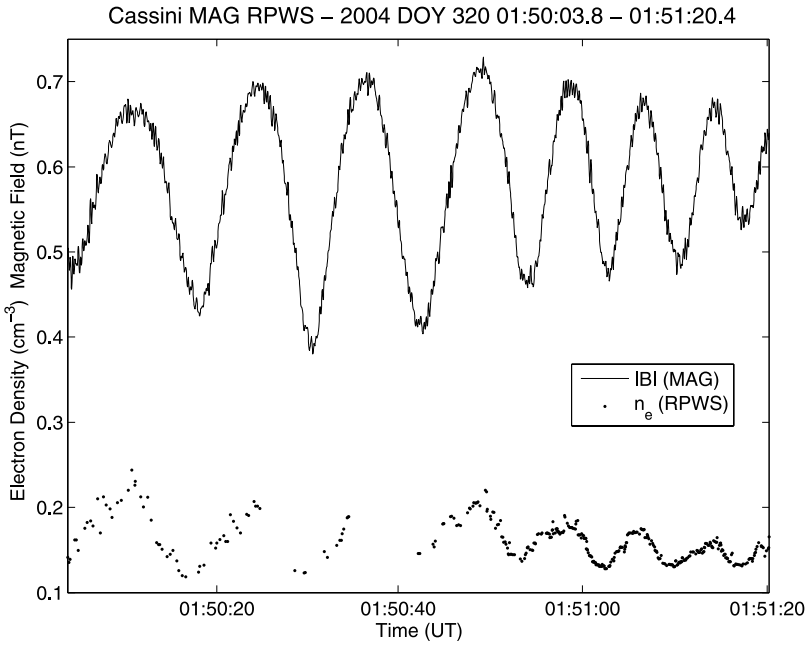

Figure 6. Magnetic field magnitude (MAG/FGM) and electron density (Radio Plasma Wave System, RPWS) for the interval 0150:03.8–0151:20.4 UT on day 320. Note the correlation between the two quantities for the wave train attached to the low-frequency steepened waves at frequencies below Ω_{H+} (located on the left), in spite of the data gaps in n_e around 0150:26 and 0150:37.

velocity is parallel to the Sun-Saturn line, the location of the foreshock boundary can be deduced using the technique described by *Greenstadt and Baum* [1986]. In this technique we used the model for Saturn's bow shock obtained by *Slavin et al.* [1985] from Voyager and Pioneer observations. This model is scaled in size by the solar wind dynamic pressure and predicts a hyperboloidal bow shock with eccentricity 1.71 and focal distance 6 R_S. We used the *Slavin et al.* [1985] model and varied the semilatus rectum L so as to coincide with the bow shock crossings by Cassini. As a result, the approximate location and shape of Saturn's bow shock for a given wave event can be determined from the bow shock crossing which is closest in time to the observations.

[24] We applied this method to the long wave train observations from 14 to 16 November 2004 (days 319–321). The closest bow shock crossing took place on 7 November 2004 (day 312) at 1243:48, and the scaling of the *Slavin et al.* [1985] model gives L = 43.84, and a resulting standoff distance of 22.18 R_S. If we assume that the shock shape and position has not changed considerably between the event and the shock crossing, we can calculate the location of the foreshock boundary by looking at the orientation of the ambient magnetic field and then estimate the distance from this boundary to the events. As a result, these waves are located approximately $\sim$50 R_S inside the foreshock. At the point of intersection (located at 3.92 R_S from the event) the angle between the magnetic field and the model shock normal is $\theta_{Bn} = 45°$.

2.2. Waves at Frequencies Above Ω_{H+}

[25] Cassini MAG measurements also revealed a second category of waves, whose frequencies are significantly higher (up to 5 times) than the local proton cyclotron frequency. These waves are not as frequent as those in the first category at least during the period of study and they tend to appear closer to the bow shock crossings. In this section we will describe two examples of observations which help understand their main experimental properties. Figure 7 shows the magnetic field magnitude and electron counts for energies below 20 keV measured by Cassini MAG and Cassini Electron Spectrometer CAPS/ELS [*Young et al.*, 2004], respectively, from 0300:00 on the 10 December until 0300:00 on the 11 December. During this period, Cassini crosses Saturn's bow shock several times. The enhancement in the magnetic field magnitude and variability, and the electron heating clearly define the excursions into the magnetosheath: 0902:43 (inbound), 1018:50 (outbound), 1255:44 (inbound), 1520:12 (outbound), 1545:03 (inbound), and 1809:31 (outbound) on 10 December, and 0002:08 (inbound) and 0022:20 (outbound) on 11 December. During this period, we identified two events labeled A and B where waves at frequencies higher than Ω_{H+} were observed. As MAG and ELS data shows, these wave events are clearly outside the bow shock. Figure 8 shows magnetic field vector measurements which illustrate examples of the waves within the A event (0705–0735 on 10 December). The waves look quasi-monochromatic and less compressive than the waves belonging to the first group, with peak-to-peak amplitudes of the order of 0.5 nT. As seen in the three oscillations around 0725, these waves develop a significant compressive component when the amplitude increases ($|\delta\mathbf{B}|/|\mathbf{B}| > 1$) and as a consequence of this, their propagation is no longer parallel, but oblique ($\theta_{kB} = 43.1 \pm 0.9°$ for the interval 0724–0727).

[26] In the spacecraft frame, these waves have periods of the order of 60 s. According to the ambient magnetic field

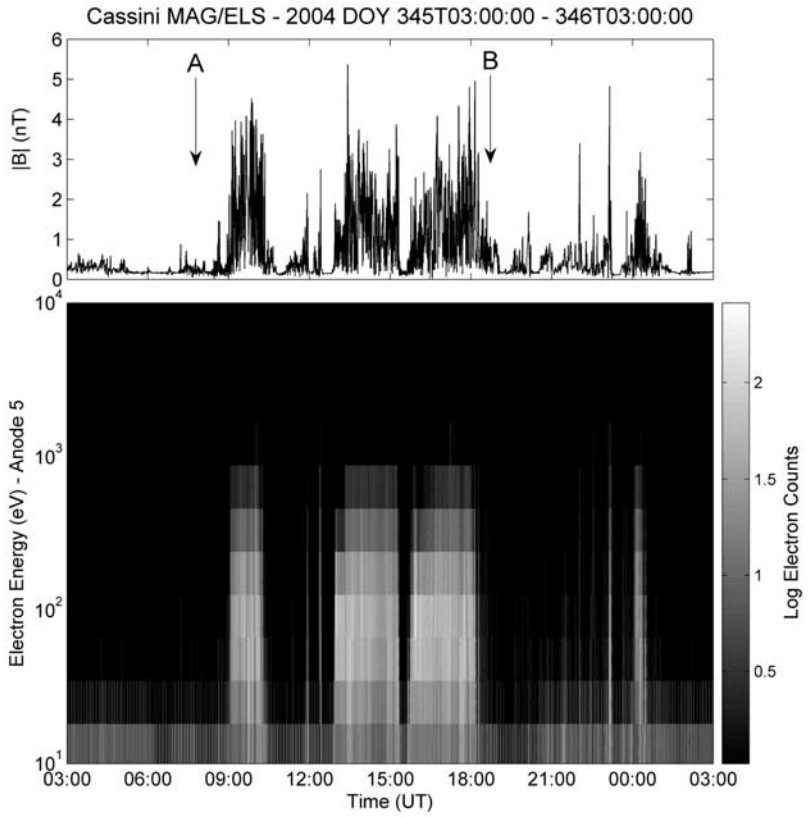

Figure 7. Magnetic field magnitude (from MAG/VHM) and electron counts for the range 10 eV to 10 KeV (from Cassini Electron Spectrometer (CAPS/ELS), Anode 5) for the interval DOY 345 0300:00 to DOY 346 0300:00. Quasi-monochromatic and steepened waves at frequencies above Ω_{H+} are observed in intervals A and B, respectively.

magnitude, this value is significantly ($\sim$ 0.2) lower than the local proton cyclotron period $T_{H+} \sim 300$ s.

[27] We analyzed the polarization of these waves using MVA. Figure 9 shows the results of the analysis for the interval 0730:33–0732:39. Figure 9a shows the magnetic field along the direction of maximum, intermediate, and minimum variance of the magnetic field. As the plot clearly shows, the amplitude of the fluctuations in B_3 ($\sim$0.1 nT) is negligible with respect to those in B_1 and B_2 ($\sim$0.5 nT). As a result, the minimum variance plane is well defined ($\lambda_2/\lambda_3 = 74.6$) and the wave is planar, as the hodogram in Figure 9b shows. The hodogram in Figure 9c reveals that the polarization on the minimum variance plane is circular, with a right-hand helicity. The angle between the mean magnetic field and the minimum variance eigenvector is $7.5° \pm 1.2°$, revealing that these waves do not propagate parallel but slightly obliquely to the ambient field. The point of magnetic connection to the shock surface containing the crossing at 0902:43, and located at 0.3 R_S, gives a shock normal angle around 41°.

[28] It is interesting to compare these events with the characteristics of the oscillations located in the interval B, closer to the outbound shock crossing at 1809:31 on 10 December. The point of connection to the shock surface containing the shock crossing at 1809:31 is located at $\sim$0.15 R_S and the shock normal angle there is around 50°. Figure 10 shows the magnetic field vector measured by MAG in KSO coordinates between 1821:00 and 1837:00. Here we find highly compressive, steepened waves with similar periods as those in the interval A for similar mean magnetic field values.

[29] Figure 11 shows the MVA results for one of the steepened wave periods. These display a very well defined minimum variance direction (λ_2/λ_3 is near 45), and the hodogram in Figure 11c shows a right-hand polarization with respect to the minimum variance direction. In this case, $\theta_{kB} \sim 80°$, which indicates a quasi-perpendicular propagation. However, an MVA analysis applied on 5 to 10 min running windows throughout the interval where these waves are observed shows that $30° < \theta_{kB} < 80°$.

[30] These steepened waves also display higher-frequency wave packets. As shown in Figure 12, these waves are very similar to those illustrated in Figures 4 and 5 (including the decrease in the periods and the left-handed polarization), with only two differences: the shorter timescale of the oscillations (of the order of 5 s), and the slightly higher θ_{kB} ($46.9 \pm 1.1°$) value. However, the latter could be a consequence of a low-frequency component in the ambient field that it is very difficult to remove. However, in opposition to the first group of waves, the polarizations of the steepened waves above Ω_{H+} and those of their associated dispersive wave trains are oppositely directed. Finally, it is worth noting that the steepened waves that we

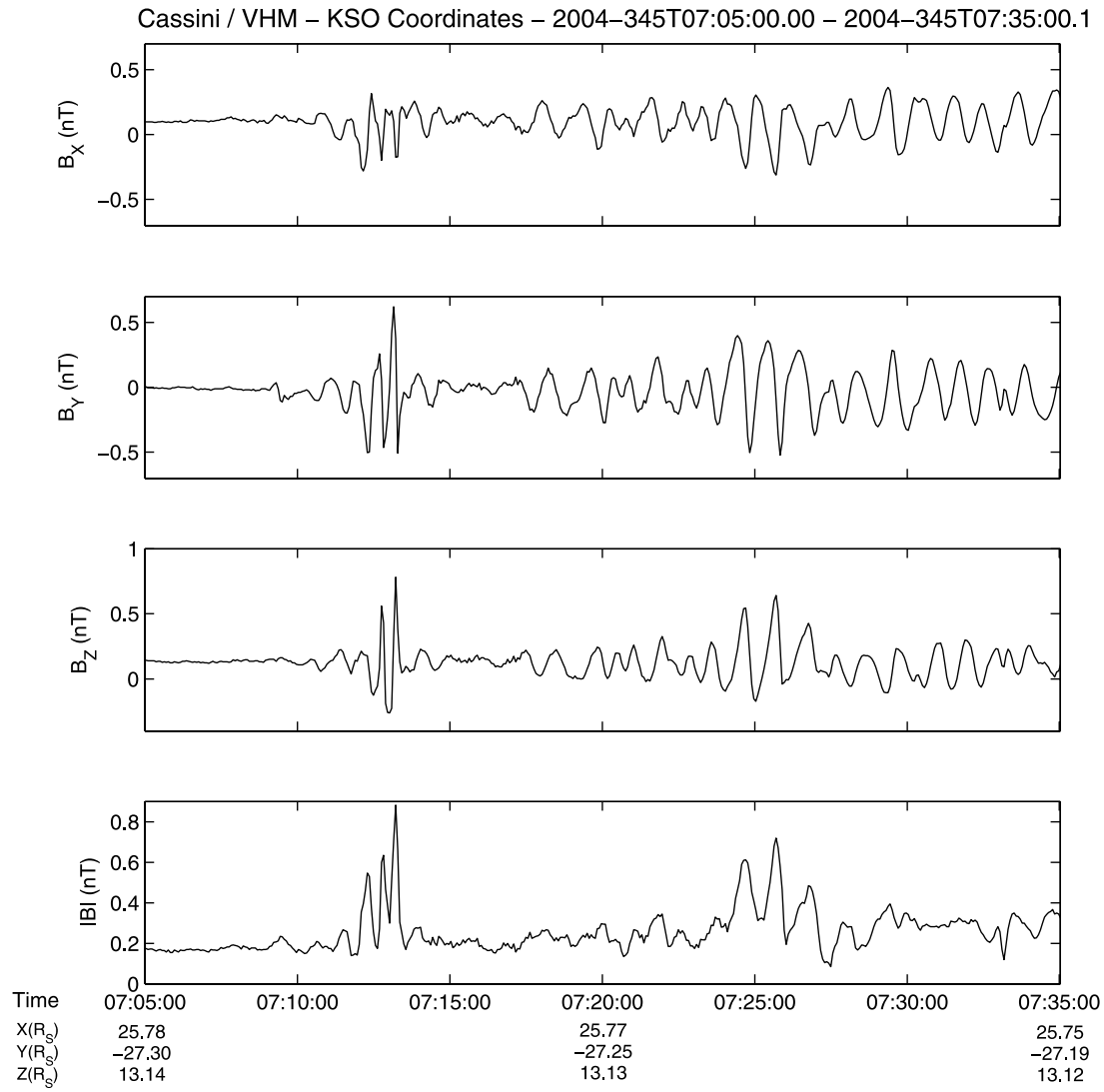

Figure 8. Cassini MAG/VHM data showing an example of quasi-monochromatic waves at frequencies above Ω_{H+} within region A in Figure 7.

see in region B eventually seem to become part of the quasi-parallel shock structure.

3. Discussion

[31] First of all, the supportive evidence of magnetic connection to Saturn's bow shock for all the events described here clearly shows that the waves are related to Saturn's foreshock. This means that they are likely to be generated from instabilities involving backstreaming particles. We will use the signatures obtained from Cassini observations and analogue measurements at Earth in an attempt to identify the types of instability that generate them. Nevertheless, a full theoretical discussion on the generation and nonlinear evolution of these waves is beyond the scope of this work.

3.1. Waves at Frequencies Below Ω_{H+}

[32] The large majority of the waves observed in this work correspond to this category. At Earth, the waves observed more frequently are the so-called "30-s waves" [*Le and Russell*, 1994]. These waves are also left-hand-polarized in the spacecraft frame and have frequencies of the order of 0.1 Ω_p in the spacecraft frame. These values are slightly smaller than those observed at Saturn (0.2–0.5 Ω_p).

[33] Cassini MAG measurements show that these waves are strongly compressive and display signatures associated to a nonlinear regime. The relative amplitude of these waves is usually high $\delta|B|/|B| > 1$ well above the values reported by *Bavassano-Cattaneo et al.* [1991], although the frequency range is similar. The remnant left-hand polarization suggests that these waves are initially fast magnetosonic (i.e., ion/ion resonant right-hand) waves propagating sunward. These waves propagate sunward at speeds (typically, Alfvén's velocity V_A) smaller than the solar wind velocity and they are carried downstream, consistent with the "inverted" polarization seen by the spacecraft. This mode can be easily become unstable in presence of cold, field aligned ion beams [*Gary*, 1993]. Interestingly, monochromatic waves with similar frequency and polarization are not observed.

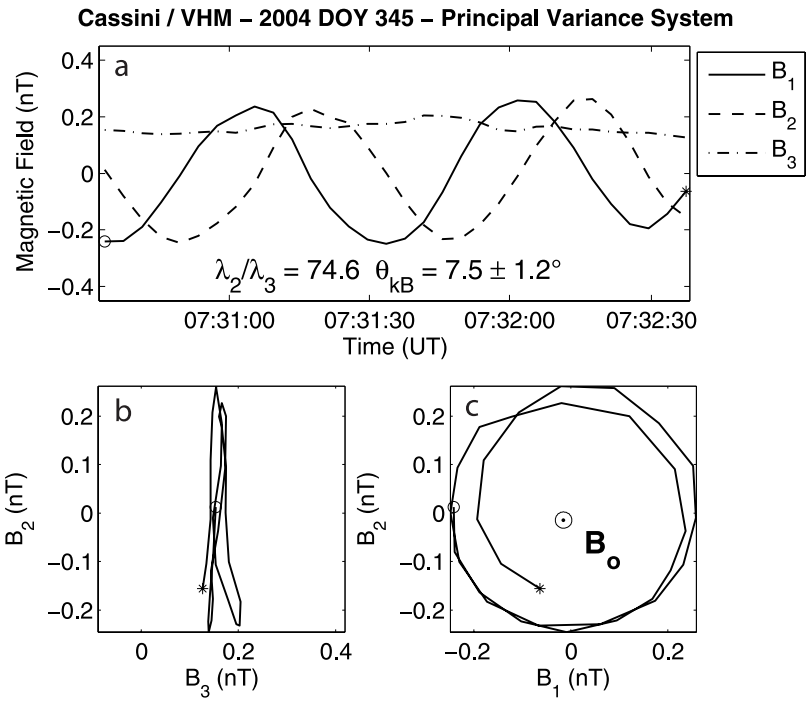

Figure 9. (a) Magnetic field components along the maximum variance direction (solid line), intermediate variance direction (dashed line), and minimum variance direction (dot-dashed line) obtained from the interval 0730:33–0732:39 UT on 10 December (day 345) 2004. (b) Hodogram showing the magnetic field in the intermediate-minimum variance plane. (c) Hodogram showing the magnetic field in the maximum-intermediate variance plane. The circle and the asterisk indicate the beginning and the end of the hodogram, respectively.

[34] Wave steepening is a result of a wave-wave interaction coupled with the dispersive nature of the solar wind plasma when the amplitude of the wave exceeds a certain threshold value. The existence of this threshold value is associated with the fact that a given wavelength can support a certain maximum amplitude before leading to harmonic excitation [*Lembège*, 1990]. During the linear phase of the wave growth, the amplitude is relatively small with respect to the threshold, and the wave's phase velocity V_{ph} does not depend on amplitude. Once the threshold is exceeded, parts of the wave with different amplitudes will have different speeds (since V_{ph} is now dependent on the amplitude). This deformation leads to the emission of higher harmonics that propagate at different phase speeds owing to the dispersive nature of the ambient plasma.

[35] The wave steepening process is limited by both dissipation and dispersion. In the case of these steepened waves and subcritical shocks, dispersion occurs first [*Mellott*, 1985], and it is responsible for the occurrence of the higher-frequency wave packet. Indeed, steepening will progress until the spatial gradient reaches the scale length $1/k_0$ at which the medium becomes dispersive. Then waves with wave numbers $k > k_0$ will travel with different phase speeds, as they "leave" the steepening front. Thus k_0 is the wave number of the wave that phase-stands with respect to the front. These "escaping" waves will form the wave train that will prevent any further steepening.

[36] The occurrence of a leading dispersive wave train as shown in Figure 3 reflects that the dispersion relation $\omega(k)$ is such that $d\omega/dk > 0$ [*Mellott*, 1985]. Furthermore, polarization of these packets and the correlation with the plasma density strongly suggest that these are whistler mode waves, whose dispersion relation (of the type $\omega \propto k^2$) satisfies this condition.

[37] Although the absence of accurate solar wind dynamic pressure measurements and a physical model of the Kronian bow shock prevents us from doing a more detailed study on the occurrence of LF waves as a function of θ_{Bn}, it is interesting to recall that these nonlinear waves are observed in periods when the IMF field is close to the nominal solar wind direction, suggesting that they populate the deep ion foreshock, that is, the region connected to the quasi-parallel shock. Bearing in mind the limitations concerning the estimation of θ_{Bn}, it is interesting to note that the amplitude of the waves in the train observed between 14 November and 16 November seems to increase significantly when $\theta_{Bn} < 25–30°$. Furthermore, the wave power decreases significantly as Cassini approaches the foreshock boundary in the early hours of 16 November. This type of behavior requires further investigation.

[38] If these waves are indeed located in the deep ion foreshock, observations at Earth suggest that the backstreaming ion distributions there should be of the diffuse type. Further comparison between MAG data and particle distributions from the Cassini ion spectrometers is needed to confirm this.

3.2. Waves at Frequencies Above Ω_{H+}

[39] The waves within this frequency range occur either as quasi-monochromatic or steepened waves. The quasi-

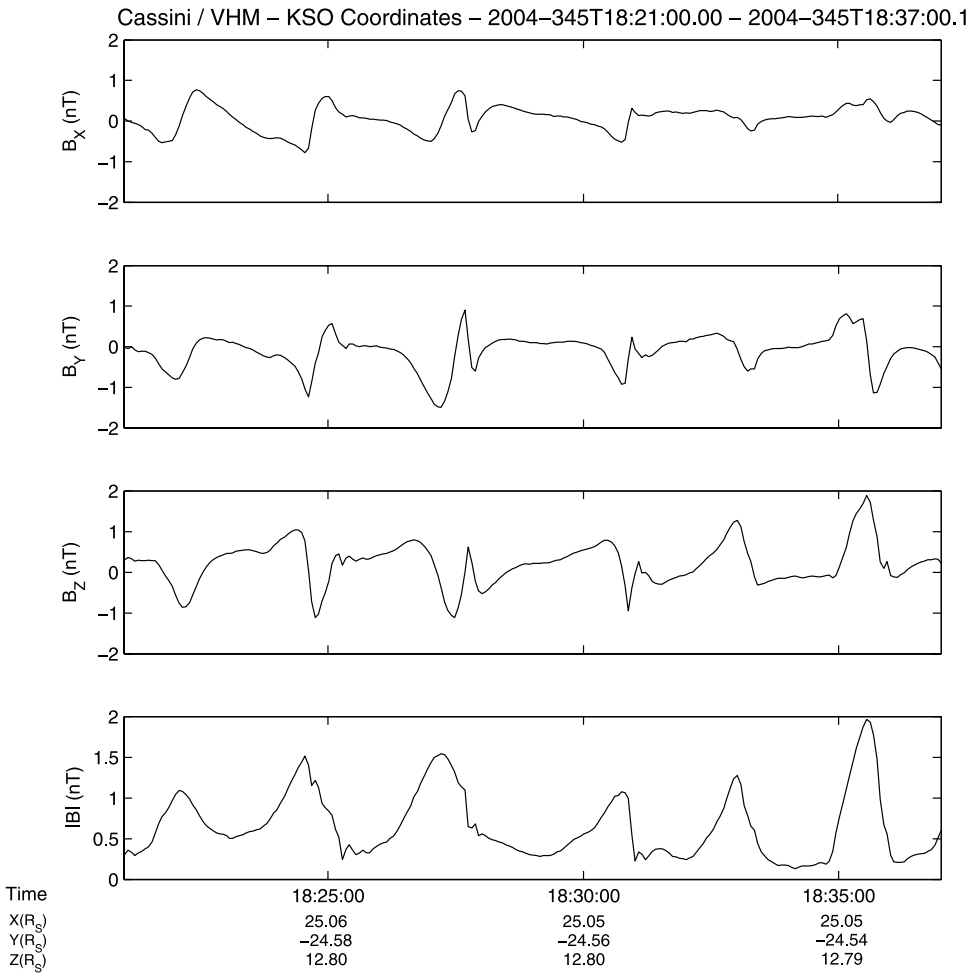

Figure 10. Cassini MAG/VHM data showing an example of steepened waves at frequencies above Ω_{H+} within region B in Figure 7.

monochromatic waves are non compressive except when the amplitude becomes important ($|\delta\mathbf{B}|/|\mathbf{B}| > 1$). This is the first time that such waves have been observed in Saturn's foreshock.

[40] Three interpretations can explain the observed right-hand polarization in the spacecraft frame: the ion/ion nonresonant instability, the ion/ion left-hand resonant instability [*Gary*, 1993] and the electromagnetic ion/ion cyclotron instability (EMIIC) [*Winske and Omidi*, 1990].

[41] The first mechanism, also known as the nonresonant fire hose instability, is excited by cool fast ion beams. According to *Le and Russell* [1994], when a beam of backstreaming ions is sufficiently fast and dense ($V_{beam} > V_A$, $n_{beam} > 0.1\ n_{SW}$, where n_{SW} is the solar wind density) this instability will excite LF waves in the magnetosonic branch which propagate in the direction opposite to the ion beam (i.e., planetward), and therefore these waves will be perceived as right-hand in the spacecraft frame. In fact, the growth rate of the nonresonant instability can be larger than that of the resonant one if $V_{beam}/V_A \gg 1$ and $n_{beam}/n_{SW} \gg 1$ [*Gary et al.*, 1984], and it is likely to be even larger if the beam is made of heavier ions [*Winske and Gary*, 1986]. However, no conclusive evidence of magnetospheric heavy ions in the upstream region has been reported so far.

[42] The second mechanism, also referred to as the Alfvén/ion cyclotron instability, arises when the backstreaming ions are hot ($V_{thermal} > V_{beam}$) [*Sentman et al.*, 1981]. This instability leads to LF left-hand waves propagating upstream from the bow shock that will appear as right-hand in the spacecraft frame, as they are convected downstream by the solar wind. This instability has a lower velocity threshold [*Gary et al.*, 1984] and has been claimed to be found in the Earth's foreshock [*Eastwood et al.*, 2003]. One potentially controversial aspect is the fact that because of the limited availability of Cassini ion data, we cannot provide evidence for such hot ion distributions.

[43] The third mechanism (EMIIC) is an instability that is generated by relatively cold ion beams and gives rise to obliquely propagating, weakly compressive Alfvèn waves. However, a parallel propagation like the one showed in Figure 9 requires β values of the order of 0.01 [*Winske and Omidi*, 1990], which are extremely low with respect to those reported at Saturn by Cassini [see *Achilleos et al.*, 2006]. Because of this, the EMIIC instability seems to be very unlikely candidate to generate these waves.

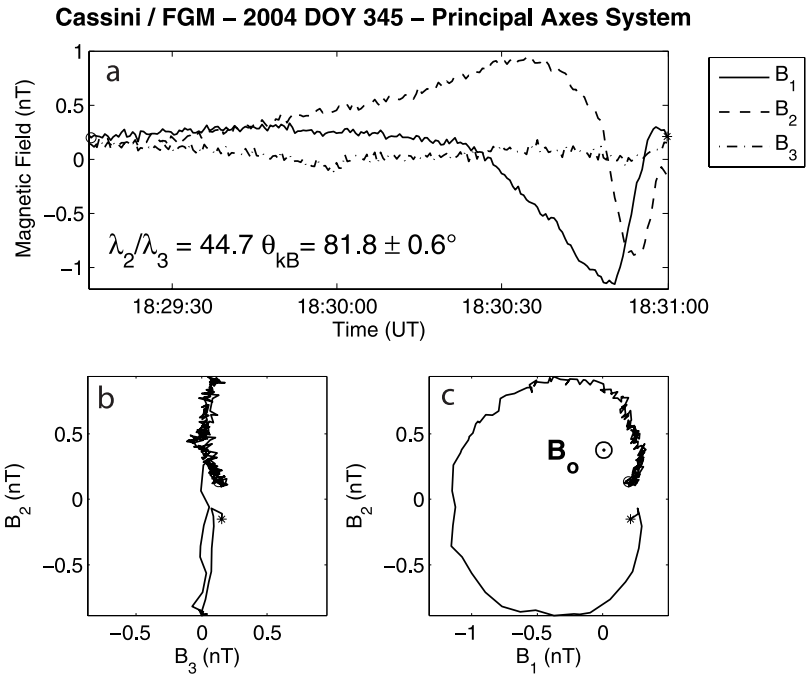

Figure 11. (a) Magnetic field components along the maximum variance direction (solid line), intermediate variance direction (dashed line), and minimum variance direction (dot-dashed line) obtained from the interval 1829:20–1431:00 UT on 10 December (day 345) 2004. (b) Hodogram showing the magnetic field in the intermediate-minimum variance plane. (c) Hodogram showing the magnetic field in the maximum-intermediate variance plane. The circle and the asterisk indicate the beginning and the end of the hodogram, respectively.

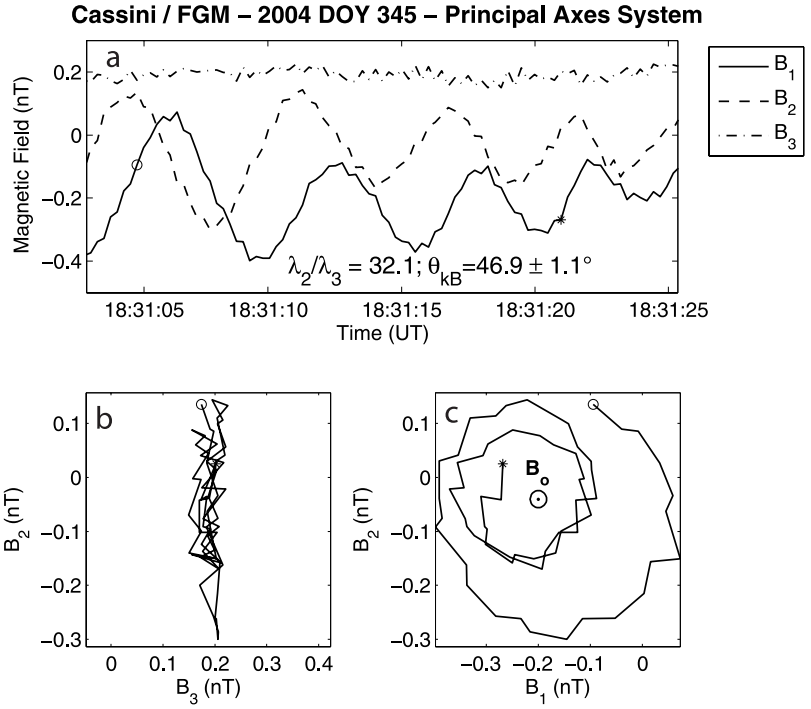

Figure 12. (a) Magnetic field components along the maximum variance direction (solid line), intermediate variance direction (dashed line), and minimum variance direction (dot-dashed line) obtained from the interval 1831:03–1831:26 UT on 10 December (day 345) 2004. (b) Hodogram showing the magnetic field in the intermediate-minimum variance plane. (c) Hodogram showing the magnetic field in the maximum-intermediate variance plane. The circle and the asterisk indicate the beginning and the end of the hodogram, respectively.

[44] Closer to the shock we find steepened, compressive waves with a similar frequency and polarization, indicating that these could represent an advanced stage of evolution of the quasi-monochromatic waves previously described. Therefore, if we assume that these two subgroups of waves are indeed related, we can study the morphology of the steepened waves to infer their propagation.

[45] Once again, the steepened waves are preceded by dispersive wave trains with similar morphology as those associated with the waves at frequencies below Ω_{H+}: decrease in the period and amplitude with increasing distance from the steepening front and left-hand polarization in the spacecraft frame. These features strongly suggest that once again, these packets correspond to the whistler mode, which has been emitted to stop the steepening process. If this is the case, the whistler wave packet is propagating sunward, but it is being swept back by the solar wind. However, as the low-frequency end of the wave packet is at rest with respect to the steepening front, the "mother wave" must also propagate toward the Sun, indicating that the nonresonant fire hose instability can be discarded.

[46] This leaves us with the ion/ion left-hand resonant instability that can indeed generate parallel propagating left-hand-polarized waves like the ones in Figure 9. However, these noncompressive Alfvèn modes have phase speeds that decrease at shorter wavelengths, so they do not have the same mechanism for steepening as the right-hand-polarized waves. This contradiction could be solved if these waves could develop a compressive component and an oblique propagation in their nonlinear stage of growth. The MVA results for the oscillations around 0725 in Figure 8 clearly reveals that these waves become compressive and obliquely propagating (with θ_{kB} values very close to the ones of the steepened waves) when their amplitude is large with respect to the linear saturation ($|\delta\mathbf{B}|/|B| = 3.1$ and $\delta|B|/|B| = 2.8$), without showing signs of steepening yet.

[47] So, it could be possible to imagine a scenario where parallel propagating Alfvèn waves are generated from the ion/ion left-hand resonant instability (assuming that there are hot beams to do it). These waves grow and diffuse the beam, and then (by either quasi-linear effects or fully nonlinear effects) they become compressive and obliquely propagating. In the kinetic Alfvèn wave regime, these waves present now whistler-like dispersion, so they can eventually steepen and emit a whistler precursor. At a later stage, and closer to the shock, these steepened waves would become SLAMS that end up being part of the shock structure, contributing to its reformation.

[48] It is interesting to notice that for these waves the period in the spacecraft frame is $\sim$0.2 times the local proton cyclotron period. In this respect and as well as in morphology and polarization, these waves are similar to the so-called 3-s waves in Earth's foreshock associated with hot backstreaming ion distributions [*Le and Russell*, 1994].

4. Conclusions

[49] We presented the first characterization of Saturn's foreshock from Cassini observations by analyzing the properties of the LF waves generated from the backstreaming ions that populate this region. As a result of a survey carried out over the first three orbits of Cassini, we have found that the LF waves concentrate around two ranges of frequencies in the spacecraft frame: one below and the other above the local proton cyclotron frequency.

[50] Most of the waves correspond to the first category. They display phase steepening and an elliptical left-handed polarization in the spacecraft frame. These waves are often accompanied by precursor whistler wave trains. These signatures suggest that these waves are ion/ion resonant right-hand (fast magnetosonic) mode waves which steepen during the nonlinear regime and emit a dispersive whistler to stop the steepening. These waves may be identified as the Kronian counterpart of the shocklets and discrete wave packets observed in the terrestrial foreshock. The orientation of the ambient magnetic field suggests that these waves are typical of the deep ion foreshock and therefore associated to diffuse backstreaming ion distributions, but evidence of such distributions has yet to be confirmed by Cassini ion instruments. No monochromatic waves with the same frequency/polarization have been observed.

[51] The waves within the second group tend to occurcloser to the bow shock and appear either as quasi-monochromatic waves or steepened waves. The quasi-monochromatic waves have a right-hand polarization in the spacecraft frame and propagate at small angles with respect to the ambient field. Some compressibility and an oblique propagation are seen for higher amplitudes. Steepened waves are observed even closer to the shock, and seem to be related to those more distant because of their helicity and frequency. The presence of what seems to be sunward propagating whistler precursors attached to the steepened wave leads to the idea that these waves are generated from the ion/ion resonant left-hand instability and propagate sunward, but the limited availability of Cassini ion data prevents us from providing evidence for the associated hot ion beams.

[52] The steepening of the initially noncompressive parallel propagating Alfvèn waves could take place if these develop a compressive component and an oblique propagation during the nonlinear regime, but this is purely speculative. A study of the compressibility [*Gary*, 1986] using high-resolution magnetic field and plasma data in order to identify these waves as Alfvènic or not is left as a future work. Nevertheless, there is direct evidence that these waves participate in the reformation of Saturn's quasi-parallel bow shock.

[53] It is still uncertain if these waves are the Kronian equivalent of the 30 s and 3s waves found in the Earth's foreshock respectively, but the ratios of their frequencies to the local proton cyclotron frequency and their polarization seem to support this idea. A future statistical study on the distribution of these waves as a function of the angle between the IMF and the Sun-Saturn direction (in absence of a reliable shock physical model) could shed some light on the veracity of this idea. A characterization of the typical energies of the ions associated with these waves and their origin is another study to undertake in the future.

[54] **Acknowledgments.** Cesar Bertucci would like to thank S. P. Gary, S. J. Schwartz, and B. Lefebvre for their useful discussions. This work has been supported by the U.K. Particle Physics and Astronomy Council (PPARC) under grant PHSP PR2170.

[55] Amitava Bhattacharjee thanks Thomas Armstrong and Jonathan Eastwood for their assistance in evaluating this paper.

References

Achilleos, N., et al. (2006), Orientation, location, and velocity of Saturn's bow shock: Initial results from the Cassini spacecraft, *J. Geophys. Res.*, *111*, A03201, doi:10.1029/2005JA011297.

Asbridge, J. R., S. J. Bame, and I. B. Strong (1968), Outward flow of protons from the Earth's bow shock, *J. Geophys. Res.*, *73*, 5777.

Bavassano-Cattaneo, M. B., P. Cattaneo, G. Moreno, and R. P. Lepping (1991), Upstream waves in Saturn's foreshock, *Geophys. Res. Lett.*, *18*, 797–800.

Bonifazi, C., and G. Moreno (1981a), Reflected and diffuse ions backstreaming from the Earth's bow shock: 1. Basic properties, *J. Geophys. Res.*, *86*, 4397–4413.

Bonifazi, C., and G. Moreno (1981b), Reflected and diffuse ions backstreaming from the Earth's bow shock: 2. Origin, *J. Geophys. Res.*, *86*, 4405–4414.

Dougherty, M. K., et al. (2004), The Cassini magnetic field investigation, *Space Sci. Rev.*, *114*(1–4), 331–383.

Eastwood, J. P., A. Balogh, E. A. Lucek, C. Mazelle, and I. Dandouras (2003), On the existence of Alfvén waves in the terrestrial foreshock, *Ann. Geophys.*, *21*(7), 1457–1465.

Feldman, W. C., R. C. Anderson, S. J. Bame, J. T. Gosling, R. D. Zwickl, and E. J. Smith (1983), Electron velocity distributions near interplanetary shocks, *J. Geophys. Res.*, *88*, 9949–9958.

Gary, S. P. (1986), Low-frequency waves in a high-beta collisionless plasma polarization, compressibility and helicity, *J. Plasma Phys.*, *35*, 431–447.

Gary, S. P. (1993), *Theory of Space Plasma Microinstabilities*, Cambridge Univ. Press, New York.

Gary, S. P., J. T. Gosling, and D. W. Forslund (1984), Erratum: Correction to "The electromagnetic ion beam instability upstream of the Earth's bow shock", *J. Geophys. Res.*, *89*(A1), 404.

Greenstadt, E. W., and L. W. Baum (1986), Earth's compressional foreshock boundary revisited observations by the ISEE 1 magnetometer, *J. Geophys. Res.*, *91*, 9001–9006.

Gurnett, D. A., et al. (2004), The Cassini Radio and Plasma Wave Investigation, *Space Sci. Rev.*, *114*(1–4), 395–463.

Hoppe, M. M., and C. T. Russell (1982), Particle acceleration at planetary bow shock waves, *Nature*, *295*, 41.

Hoppe, M. M., C. T. Russell, T. E. Eastman, and L. A. Frank (1982), Characteristics of the ULF waves, *J. Geophys. Res.*, *87*, 643–650.

Le, G., and C. T. Russell (1994), The morphology of ULF waves in the Earth's foreshock, in *Solar Wind Sources of Magnetospheric Ultra-Low-Frequency Waves*, *Geophys. Monogr. Ser.*, vol. 81, edited by M. J. Engebretson, K. Takahashi, and M. Scholer, pp. 87–98, AGU, Washington, D. C.

Lembège, B. (1990), Numerical simulations of collisionless shocks, in *Physical Processes in Hot Cosmic Plasmas*, edited by W. Brinkman et al., pp. 81–139, Springer, New York.

Mazelle, C., et al. (2003), Production of gyrating ions from nonlinear wave-particle interaction upstream from the Earth's bow shock: A case study from Cluster-CIS, *Planet. Space Sci.*, *51*(12), 785–795.

Mellott, M. M. (1985), Subcritical collisionless shock waves, in *Collisionless Shocks in the Heliosphere: Reviews of Current Research*, *Geophys. Monogr. Ser.*, vol. 35, edited by R. G. Stone and B. T. Tsurutani, pp. 131–140, AGU, Washington, D. C.

Meziane, K., et al. (2004), Bow shock specularly reflected ions in the presence of low-frequency electromagnetic waves: A case study, *Ann. Geophys.*, *22*(7), 2325–2335.

Narita, Y., K.-H. Glassmeier, K.-H. Fornaçon, I. Richter, S. Schäfer, U. Motschmann, I. Dandouras, H. Rème, and E. Georgescu (2006), Low-frequency wave characteristics in the upstream and downstream regime of the terrestrial bow shock, *J. Geophys. Res.*, *111*, A01203, doi:10.1029/2005JA011231.

Paschmann, G., N. Sckopke, J. R. Asbridge, S. J. Bame, and J. T. Gosling (1980), Energization of solar wind ions by reflection from the Earth's bow shock, *J. Geophys. Res.*, *85*, 4689–4693.

Pinçon, J. L., and U. Motschmann (1998), Multispacecraft filtering: General framework, in *Analysis Methods for Multispacecraft Data*, edited by G. Paschmann and P. W. Daly, *Sci. Rep. SR-001*, pp. 65–78, Int. Space Sci. Inst., Bern, Switzerland.

Russell, C. T. (1985), Planetary bow shocks, in *Collisionless Shocks in the Heliosphere: Reviews of Current Research*, *Geophys. Monogr. Ser.*, vol. 35, edited by R. G. Stone and B. T. Tsurutani, pp. 109–130, AGU, Washington, D. C.

Russell, C. T., D. D. Childers, and P. J. Coleman Jr. (1971), Ogo 5 observations of upstream waves in the interplanetary medium: Discrete wave packets, *J. Geophys. Res.*, *76*, 845.

Schwartz, S. J., and D. Burgess (1991), Quasi-parallel shocks: A patchwork of three-dimensional structures, *Geophys. Res. Lett.*, *18*, 373–376.

Schwartz, S. J., D. Burgess, W. P. Wilkinson, R. L. Kessel, M. Dunlop, and H. Lühr (1992), Observations of short-large amplitude magnetic structures at a quasi parallel shock, *J. Geophys. Res.*, *97*(A4), 4209–4227.

Sentman, D. D., J. P. Edmiston, and L. A. Frank (1981), Instabilities of low frequency, parallel propagating electromagnetic waves in the Earth's foreshock region, *J. Geophys. Res.*, *86*, 7487–7497.

Slavin, J. A., E. J. Smith, J. R. Spreiter, and S. S. Stahara (1985), Solar wind flow about the outer planets: Gas dynamic modeling of the Jupiter and Saturn bow shocks, *J. Geophys. Res.*, *90*, 6275–6286.

Sonnerup, B. U. O., and M. Schreible (1998), Minimum and maximum variance analysis, in *Analysis Methods for Multispacecraft Data*, edited by G. Paschmann and P. W. Daly, *Sci. Rep. SR-001*, pp. 185–220, Int. Space Sci. Inst., Bern, Switzerland.

Thomsen, M. F., J. T. Gosling, S. J. Bame, W. C. Feldman, G. Paschmann, and N. Sckopke (1983), Field-aligned ion beams upstream of the Earth's bow shock: Evidence for a magnetosheath source, *Geophys. Res. Lett.*, *10*, 1207–1210.

Tokar, R. L., et al. (2006), The interaction of the atmosphere of Enceladus with Saturn's plasma, *Science*, *311*(5766), 1409–1412.

Winske, D., and S. P. Gary (1986), Electromagnetic instabilities driven by cool heavy ion beams, *J. Geophys. Res.*, *91*, 6825–6832.

Winske, D., and N. Omidi (1990), Electromagnetic ion/ion cyclotron instability, *Geophys. Res. Lett.*, *17*(12), 2297–2300.

Young, D. T., et al. (2004), Cassini plasma spectrometer investigation, *Space Sci. Rev.*, *114*(1–4), 1–112.

Young, D. T., et al. (2005), Composition and dynamics of plasma in Saturn's magnetosphere, *Science*, *307*(5713), 1262–1266, doi:10.1126/science.1106151.

N. Achilleos, C. Bertucci, and M. K. Dougherty, Space and Atmospheric Physics Group, Imperial College London, Prince Consort Rd., London SW7 2BZ, UK. (c.bertucci@imperial.ac.uk)

G. B. Hospodarsky and W. Kurth, University of Iowa, Iowa City, IA 52242, USA.

C. Mazelle, Centre d'Etude Spatiale des Rayonnements, CNRS, Université Paul Sabatier, 9 avenue du Colonel Roche, 44346 31028 Toulouse, Cedex 4, France.

M. Thomsen, Los Alamos National Laboratory, Los Alamos, NM 87545, USA.